



## Article

# Fractal Evolution Characteristics on the Three-Dimensional Fractures in Coal Induced by CO<sub>2</sub> Phase Transition Fracturing

Zhen Zhang <sup>1,2</sup>, Gaofeng Liu <sup>1,\*</sup>, Jia Lin <sup>2</sup> , George Barakos <sup>2</sup> and Ping Chang <sup>2,\*</sup>

<sup>1</sup> School of Resources & Environment, Henan Polytechnic University, Jiaozuo 454003, China; zhen.zhang2@curtin.edu.au

<sup>2</sup> WA School of Mines: Minerals, Energy and Chemical Engineering, Curtin University, Kalgoorlie, WA 6430, Australia; jia.lin@curtin.edu.au (J.L.); george.barakos@curtin.edu.au (G.B.)

\* Correspondence: 10460100128@hpu.edu.cn (G.L.); ping.chang@curtin.edu.au (P.C.)

**Abstract:** To analyze the transformed effect of three-dimensional (3D) fracture in coal by CO<sub>2</sub> phase transition fracturing (CO<sub>2</sub>-PTF), the CO<sub>2</sub>-PTF experiment under a fracturing pressure of 185 MPa was carried out. Computed Tomography (CT) scanning and fractal theory were used to analyze the 3D fracture structure parameters. The fractal evolution characteristics of the 3D fractures in coal induced by CO<sub>2</sub>-PTF were analyzed. The results indicate that the CO<sub>2</sub> phase transition fracturing coal has the fracture generation effect and fracture expansion-transformation effect, causing the maximum fracture length, fracture number, fracture volume and fracture surface area to be increased by 71.25%, 161.94%, 3970.88% and 1330.03%. The fractal dimension ( $D_N$ ) for fracture number increases from 2.3523 to 2.3668, and the fractal dimension ( $D_V$ ) for fracture volume increases from 2.8440 to 2.9040. The early dynamic high-pressure gas jet stage of CO<sub>2</sub>-PTF coal influences the fracture generation effect and promotes the generation of 3D fractures with a length greater than 140 μm. The subsequent quasi-static high-pressure gas stage influences the fracture expansion-transformation effect, which promotes the expansion transformation of 3D fractures with a length of less than 140 μm. The 140 μm is the critical value for the fracture expansion-transformation effect and fracture generation effect. Five indicators are proposed to evaluate the 3D fracture evolution in coal caused by CO<sub>2</sub>-PTF, which can provide theoretical and methodological references for the study of fracture evolution characteristics of other unconventional natural gas reservoirs and their reservoir stimulation.

**Keywords:** CO<sub>2</sub> phase transition fracturing; three dimensional fracture; fractal dimension; CT scanning; fracture evolution



**Citation:** Zhang, Z.; Liu, G.; Lin, J.; Barakos, G.; Chang, P. Fractal Evolution Characteristics on the Three-Dimensional Fractures in Coal Induced by CO<sub>2</sub> Phase Transition Fracturing. *Fractal Fract.* **2024**, *8*, 273. <https://doi.org/10.3390/fractalfract8050273>

Academic Editor: Francesco Marotti De Sciarra

Received: 10 April 2024

Revised: 30 April 2024

Accepted: 1 May 2024

Published: 4 May 2024



**Copyright:** © 2024 by the authors. Licensee MDPI, Basel, Switzerland. This article is an open access article distributed under the terms and conditions of the Creative Commons Attribution (CC BY) license (<https://creativecommons.org/licenses/by/4.0/>).

## 1. Introduction

As an important unconventional natural gas energy, the efficient development and utilization of coalbed methane (CBM) cannot only provide clean fuel, but also help reduce coal and gas outburst disasters, and alleviate the greenhouse effect [1–3]. However, low permeability is one of the key factors restricting the efficient development of CBM [4–6]. Therefore, a variety of technologies that enhance gas drainage and eliminate coal and gas outbursts have been developed, but different technologies are suitable for coal seams and mining areas with different gas geological conditions [7,8]. The research and development of safe, effective, economical and highly applicable permeability-enhanced technology is one of the main research contents and major needs in the field of coal and gas co-mining research.

CO<sub>2</sub> phase transition fracturing (CO<sub>2</sub>-PTF) technology originated from the CARDOX technology invented in the United States in 1914 [9]. The CO<sub>2</sub>-PTF technology or CARDOX technology is a non-explosive physical blasting technology that uses the high-pressure gas expansion energy generated by the heating and expansion of liquid CO<sub>2</sub> to act on the coal or rock, causing the coal or rock to fracture [10]. The energy analysis indicates that CO<sub>2</sub>

undergoes a transformation from the liquid to the supercritical and gaseous state, 1 kg of liquid CO<sub>2</sub> undergoes phase change and the produced energy is equivalent to 397 g of TNT explosive [11]. The field applications in coalmines show that CO<sub>2</sub>-PTF is a new reservoir stimulation method for enhancing permeability and eliminating gas outbursts, which has unique technical advantages, such as high safety performance and avoiding the negative effects of hydraulic measures [12–14].

Coal is a multi-scale pore–fracture media, and its pore–fracture structure characteristics and connectivity directly control the CBM desorption, diffusion and seepage [15–17]. In recent years, the transformation effect of CO<sub>2</sub>-PTF on the pore–fracture structure (gas migration channel) of coal has attracted the attention of scholars. In terms of pore transformation by CO<sub>2</sub>-PTF, Bai et al. found that the coal pore volume with pore diameter greater than 1 μm increases after CO<sub>2</sub>-PTF [18]. The study by Xia et al. showed that the pore volume and average pore diameter of coal increased, and the pore fractal dimension decreased after CO<sub>2</sub>-PTF [19]. Recent studies have indicated that CO<sub>2</sub>-PTF mainly affects pores with pore diameters larger than 2 nm, and the mesopore fractal dimension is reduced [20]. In terms of fracture transformation by CO<sub>2</sub>-PTF, Cao et al. found that the macroscopic fractures with a length of 1–3 m were produced by on-site monitoring after CO<sub>2</sub>-PTF [21], and the fractured coal sample by CO<sub>2</sub>-PTF is further observed by Scanning Electron Microscope (SEM), which found a large number of tri-radial wing micro-fractures and damage marks [22]. Liu and Liao et al. used the fracture fractal theory to calculate the fractal dimension of the two-dimensional (2D) fracture observed by SEM after CO<sub>2</sub>-PTF, and the fractal dimension for 2D fracture increased [23,24].

In summary, at this stage, the pore structure scale of coal transformed by CO<sub>2</sub>-PTF has been revealed, and the fractal theory is widely used to characterize the complexity of the pore–fracture structure in coal. However, the related research on the fracture structure induced by CO<sub>2</sub> phase transition fracturing coal (CO<sub>2</sub>-PTF coal) mainly focuses on the 2D fracture by macroscopic monitoring and SEM observation. The distribution of fractures in coal has obvious three-dimensional (3D) structural characteristics of length, aperture and height, and fracture volume comprehensively reflects fracture length, aperture and height [25–27]. The fracture surface area is the total area of the internal surface of the 3D fractures in coal [28,29]. Therefore, the number, length, volume and surface area of fractures are key parameters that reflect the 3D fractures [29–31]. The current research on the 2D fracture structure of CO<sub>2</sub>-PTF coal is not enough to fully reveal the 3D fracture evolution characteristics of CO<sub>2</sub>-PTF coal. CT scanning is a non-destructive technology, and can accurately characterize 3D fracture in coal [32,33], which provides technical support for analyzing the 3D fracture evolution of CO<sub>2</sub>-PTF coal.

Therefore, this paper carried out the CO<sub>2</sub>-PTF coal experiment, the CT scanning and fractal theory were applied to research the 3D fracture evolution characteristics of CO<sub>2</sub>-PTF coal, and the transformation effect of CO<sub>2</sub>-PTF on the 3D fracture was analyzed. This study further reveals the mechanism of coal seam transformation caused by CO<sub>2</sub>-PTF, provides new evaluation and analysis methods for studying the effect of CO<sub>2</sub>-PTF, and is conducive to further improving the reservoir stimulation theory of CO<sub>2</sub>-PTF coal.

## 2. Sample and Experimental

### 2.1. Samples

The experimental samples are collected from the J<sub>15</sub> coal seam in Pingdingshan No. 8 Coalmine, Henan province. The coal sample is bright, showing layered and massive structures, the original band structure is well preserved and the bedding is visible. The dry ash-free volatile content of the sample is 24.91%, and the maximum vitrinite reflectance is 1.22%. After the coal samples are collected, they are sealed, packaged and transported to the laboratory, where a linear cutting machine is used to prepare the coal pillar with a diameter ( $\Phi$ ) of 50 mm and length of 75 mm for the CO<sub>2</sub>-PTF experiment.

## 2.2. CO<sub>2</sub> Phase Change Fracturing Experiment

The experimental system for CO<sub>2</sub>-PTF coal is shown in Figure 1. The experimental system mainly includes the CO<sub>2</sub>-PTF device composed of liquid CO<sub>2</sub>, a heater, a pressure-controlled bursting disc, an external test pipe of the CO<sub>2</sub>-PTF device and a test holder (the test holder is facing the discharge port of the CO<sub>2</sub>-PTF). The main experiment process of the CO<sub>2</sub>-PTF coal is as follows: (1) select the pressure-controlled bursting disc of 185 MPa, assemble the CO<sub>2</sub>-PTF device and fill it with liquid CO<sub>2</sub>; (2) fix the external test pipe of the CO<sub>2</sub>-PTF device on the bracket in safety experimental chamber; (3) put the CO<sub>2</sub>-PTF device into the external test pipe, adjust the discharge port of the CO<sub>2</sub>-PTF so that it faces the test holder; (4) connect the wire of CO<sub>2</sub>-PTF device, close the external test pipe, close the safety experimental chamber, start the heater and then conduct CO<sub>2</sub>-PTF coal experiment; and (5) remove the test holder and take out the coal sample. The coal is labeled PR before CO<sub>2</sub>-PTF, and the coal is labeled PF after CO<sub>2</sub>-PTF.

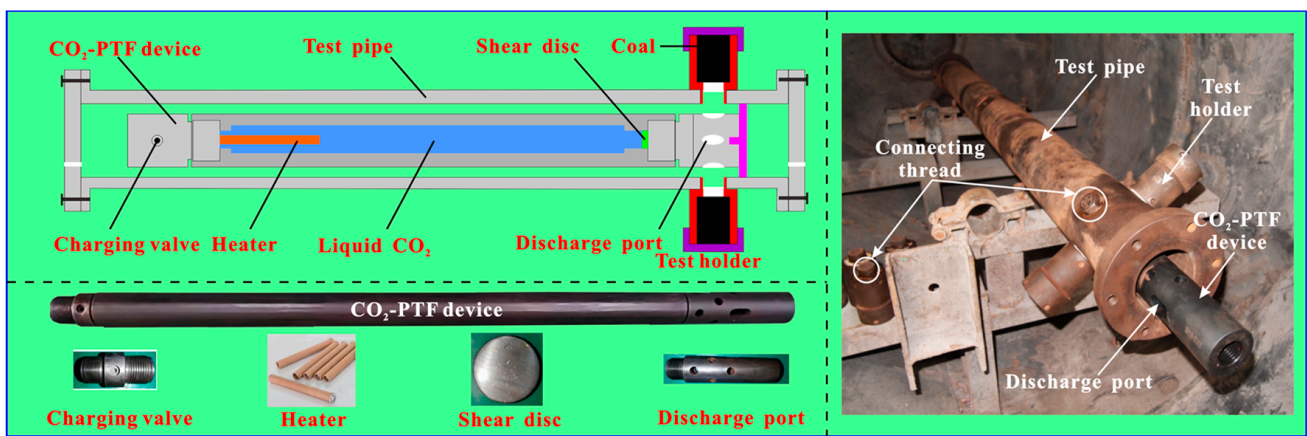


Figure 1. Experimental system of CO<sub>2</sub> phase transition fracturing.

## 2.3. CT Scanning Measurement

CT scanning technology can obtain the internal structure information of coal or rock without damaging the internal structure. The instrument used in this CT scan is GE's Phoenix v|tome|x s, and the coal sample CT scanning process is shown in Figure 2. The main parameters of CT scanning are a resolution of 30.4  $\mu\text{m}$ , scanning voltage of 200 kV, scanning current of 170  $\mu\text{A}$ , and exposure time of 500 ms, and 2467 slices of 1611  $\times$  1611 pixels are obtained for each scanning.

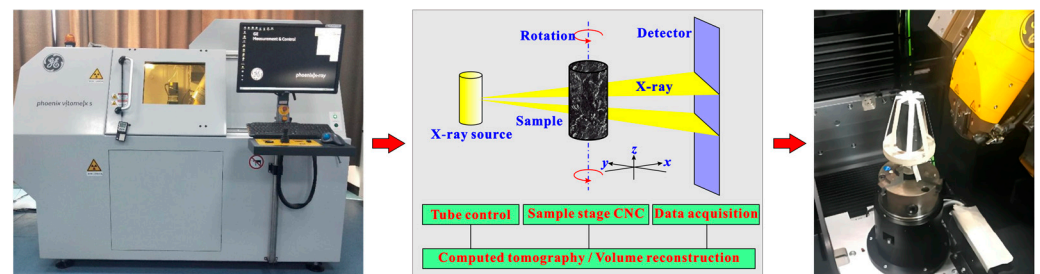


Figure 2. CT scanning of samples.

Here, to facilitate our analysis of the 3D fracture evolution characteristics of coal induced by CO<sub>2</sub>-PTF. Before CO<sub>2</sub>-PTF, CT scanning was performed on the coal sample used for the CO<sub>2</sub>-PTF experiment to obtain the original fracture structure. After CO<sub>2</sub>-PTF, the CT scanning was performed on the coal sample again to obtain the internal fracture structure.

### 3. Fractal Dimension Calculation for 3D Fracture

The fractal dimension is usually used to quantitatively describe the complexity of complex and irregular structures [34–36]. The fractal dimension  $D_N$  for 3D fracture number and fractal dimension  $D_V$  for 3D fracture volume in this research are applied to characterize the fracture complexity of CO<sub>2</sub>-PTF coal.

#### 3.1. Fractal Dimension Calculation for 3D Fracture Number

The calculation principle of the fractal dimension  $D_N$  for 3D fracture number is as follows: The number of fractures of the fracture length greater than  $L_i$  is recorded as  $N(L_i)$ , the fractal scaling relationship between  $N(L_i)$  and  $L_i$  satisfies the Equation (1) [37,38]. Taking the logarithm of  $N(L_i)$  and  $L_i$  and drawing the relation between  $\log N(L_i)$  and  $\log L_i$ , we obtain the absolute value of the slope of the line by the linear regression analysis, which is the fractal dimension  $D_N$  for 3D fracture number, as shown the Equation (2).

$$N(L_i) \propto L_i^{-D_N} \quad (1)$$

$$\log N(L_i) = -D_N \log L_i + C_1 \quad (2)$$

where  $L_i$  is the fracture length;  $N(L_i)$  is the number of fractures with the fracture length greater than  $L_i$ ;  $D_N$  is the fractal dimension for the fracture number;  $C_1$  is a fitting constant.

#### 3.2. Fractal Dimension Calculation for 3D Fracture Volume

The fracture volume  $V$  and surface area  $A$  are obtained based on CT scanning, and they satisfy the fractal scaling relationship of Equation (3) [39]. Taking the logarithm of both sides of Equation (3), the fractal dimension  $D_V$  for 3D fracture volume can be calculated by Equation (4).

$$A^{1/D_V} \propto V^{1/3} \quad (3)$$

$$\log A = (D_V/3) \log V + C_2 \quad (4)$$

where  $A$  is the surface area of the fracture;  $V$  is the volume of the fracture;  $D_V$  is the fractal dimension for the 3D fracture volume;  $C_2$  is a fitting constant.

## 4. Results

### 4.1. 2D Fractures

Figure 3 indicates the fractures in the 2D slice before and after CO<sub>2</sub>-PTF coal. Before CO<sub>2</sub>-PTF, there are no obvious large fractures inside the coal sample PR. The aperture of some original fractures is small and the connectivity of the fractures is poor (Figure 3a,b). After CO<sub>2</sub>-PTF, the obvious fracture network is generated in the coal sample PF, and the connectivity between fractures is enhanced. Furthermore, there are some new fracture structures formed from CO<sub>2</sub>-PTF coal. Large damage marks (DM) are formed and the four-radial-wing (FRW) fractures extending in four directions is generated around the large damage marks in the middle of the coal sample PF (Figure 3c,d). Some small damage marks and radial fractures are also formed in the coal sample PF (Figure 3c,d). Cao et al. also found that CO<sub>2</sub>-PTF promotes the formation of damage marks and tri-radial-wing (TRW) fractures (the three single fractures initiated from one point) by SEM observations [22]. In this study, the radial fractures formed by CO<sub>2</sub>-PTF include not only tri-radial-wing (TRW) fractures, but also four-radial-wing (FRW) fractures (the four single fractures initiated from one point) (Figure 3c,d).

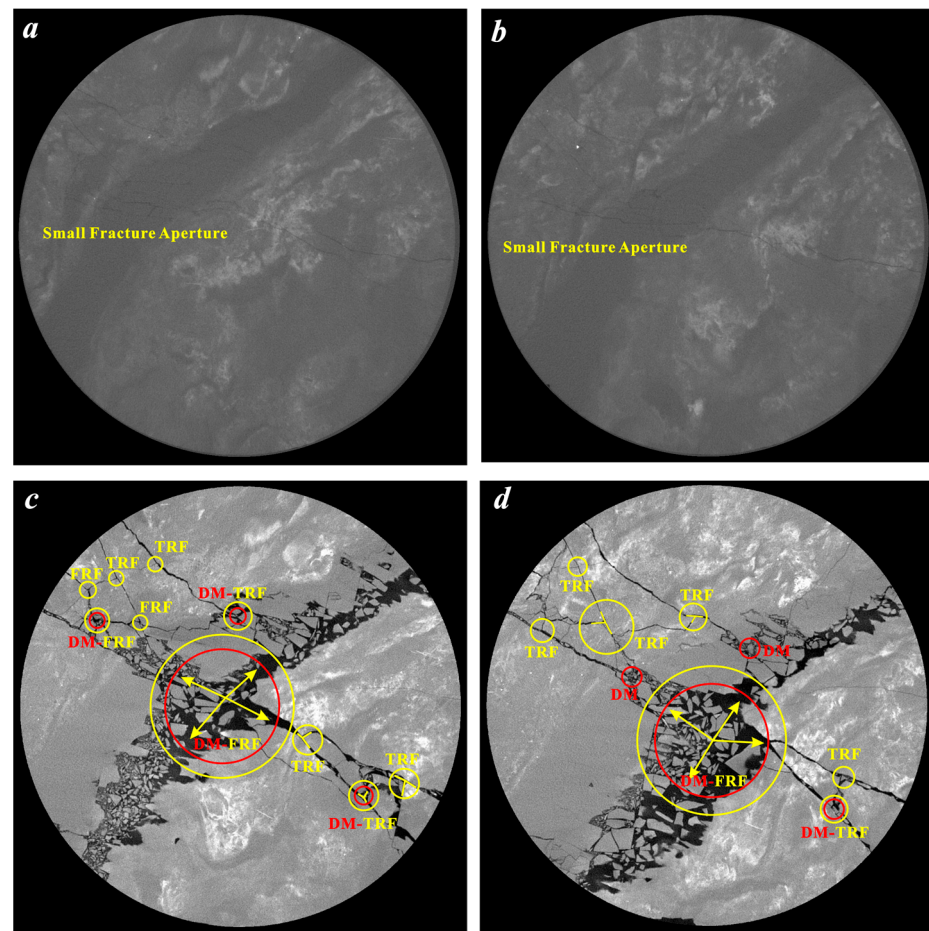


**Figure 3.** 2D Fractures induced by CO<sub>2</sub>-PTF coal: (a,b) are the 2D fractures of coal PR, (c,d) are the 2D fractures of coal PF.

Figure 3 further shows that the 2D fractures on different slices of the same sample are obviously different. Therefore, the 2D fracture can only reflect the local fracture evolution. The fractures in coal have obvious 3D characteristics [40–42]. To further truly reflect the fracture evolution of CO<sub>2</sub>-PTF coal, it is necessary to perform 3D reconstruction of the 2D slices.

#### 4.2. 3D Reconstruction of Fractures

The 2D slices obtained from the CT scanning were filtered and denoised, and subjected to threshold segmentation. The VG Studio MAX 3.0 image processing software from the Volume Graphics company (Heidelberg, Germany) was used to visualize the 3D reconstruction of the processed 2D slices of coal samples. The pore/inclusion analysis module was used to extract and analyze the defects or fractures in coal samples. The detected fractures were color-coded and visualized, and the fracture structural parameters were calculated, mainly including fracture number, length, volume and surface area.

Figure 4 shows the 3D fracture of the coal sample from 3D reconstruction before and after CO<sub>2</sub>-PTF. Before CO<sub>2</sub>-PTF, the fracture rendering color inside the coal sample PR is mainly green and blue (Figure 4a,b), the fracture volume is small and the connectivity between fractures is poor. After CO<sub>2</sub>-PTF, the complex fracture network is formed inside the coal sample PF, and the fracture rendering color is mainly red (Figure 4c,d). The fracture volume increases, and the connectivity between the fractures is enhanced. Furthermore, compared with the 3D fracture in coal sample PR, the 3D fractures in coal sample PF after CO<sub>2</sub>-PTF have obvious longitudinal continuity. This is mainly due to the high-pressure CO<sub>2</sub>

flow generated by CO<sub>2</sub>-PTF that acts on the top of the coal sample, prompting the fractures in the coal sample to expand longitudinally, forming the complex fracture network.

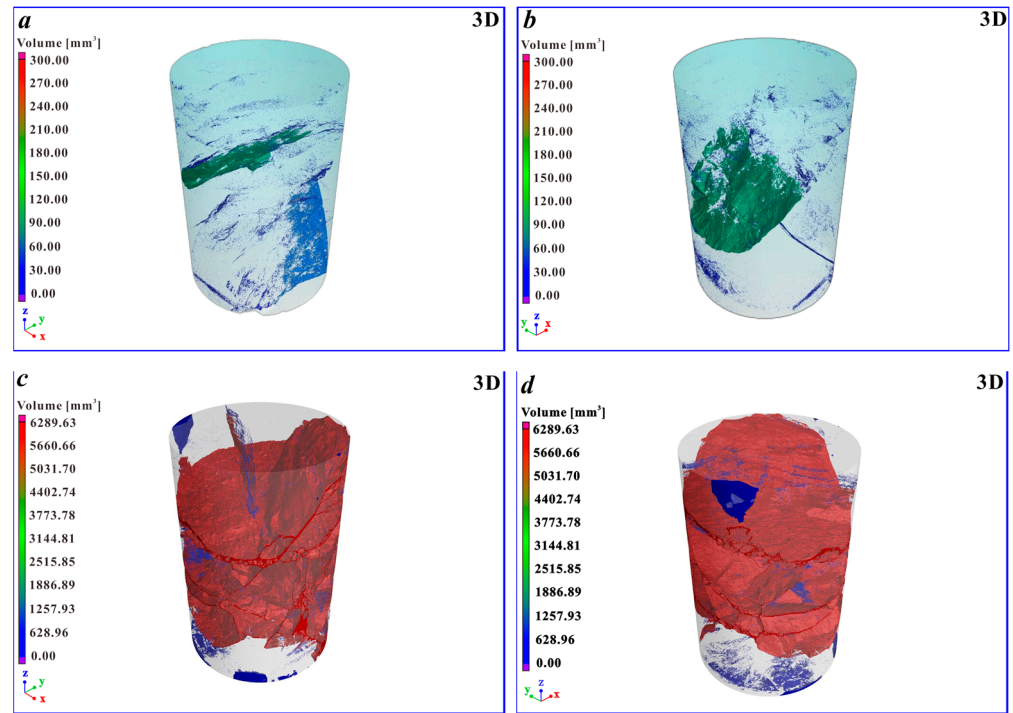


**Figure 4.** 3D Fracture in coal before and after CO<sub>2</sub>-PTF: (a,b) are the 3D fractures of coal PR, (c,d) are the 3D fractures of coal PF.

### 4.3. Fractal Dimension for 3D Fracture

#### 4.3.1. Estimation of the Fractal Dimension $D_N$ for 3D Fracture Number

Figure 5 shows that  $\log N(L_i)$  and  $\log L_i$  have an obvious linear relationship, and the correlation coefficient  $R^2$  is greater than 0.99, indicating that the number distribution of the 3D fractures inside the coal sample has obvious fractal characteristics. Before CO<sub>2</sub>-PTF, the fractal dimension  $D_N$  for 3D fracture number is 2.3523. After CO<sub>2</sub>-PTF, the fractal dimension  $D_N$  for the 3D fracture number is 2.3668.

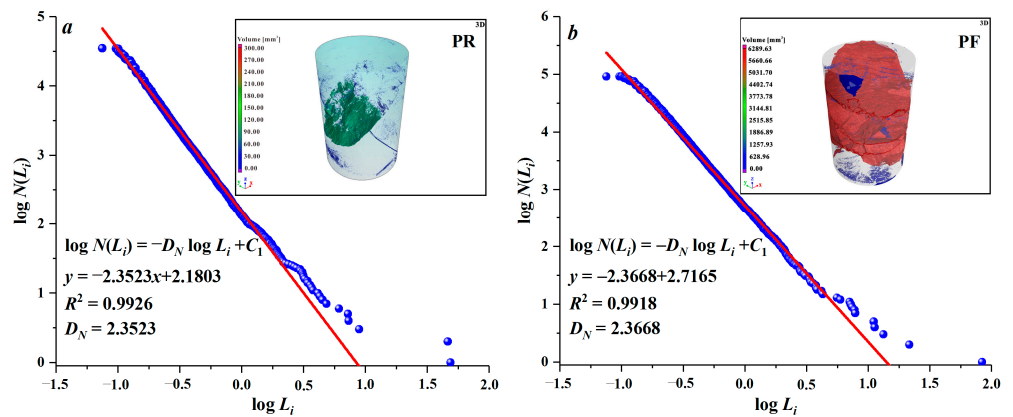


**Figure 5.** Fractal dimension  $D_N$  for 3D fracture number: (a) PR, (b) PF.

#### 4.3.2. Estimation of the Fractal Dimension $D_V$ for 3D Fracture Volume

The fracture surface area  $A$  and volume  $V$  are fitted by Equation (4) to obtain the fractal dimension  $D_V$  for 3D fracture volume. Figure 6 shows that  $\log A$  and  $\log V$  have an obvious linear relationship, and the correlation coefficient  $R^2$  is greater than 0.98, reflecting that

3D fracture volume distribution inside the coal sample has obvious fractal characteristics. After CO<sub>2</sub>-PTF, the fractal dimension  $D_V$  increases from 2.8440 to 2.9040.

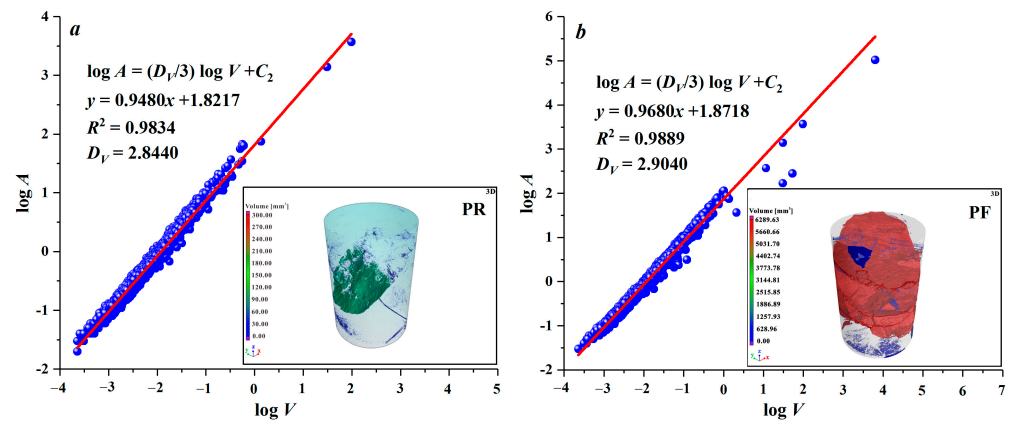


**Figure 6.** Fractal dimension  $D_V$  for 3D fracture volume: (a) PR, (b) PF.

#### 4.4. 3D Fracture Structure Variation Induced by CO<sub>2</sub>-PTF Coal

According to the 3D fracture reconstruction from CT scanning in Section 4.2, the 3D fracture structure parameters before and after CO<sub>2</sub>-PTF are shown in Figure 7. After CO<sub>2</sub>-PTF, the maximum fracture length in the coal sample increases from 48.90 mm to 83.74 mm, with an increased rate of 71.25% (Figure 7a). The fracture number increases from 35,183 to 92,159, with an increased rate of 161.94% (Figure 7b). The fracture volume  $V$  increases from 158.12 mm<sup>3</sup> to 6436.87 mm<sup>3</sup>, with an increased rate of 3970.88% (Figure 7c). The fracture surface area  $A$  increases from 7733.05 mm<sup>2</sup> to 110,585.06 mm<sup>2</sup>, an increase of 1330.03% (Figure 7d).

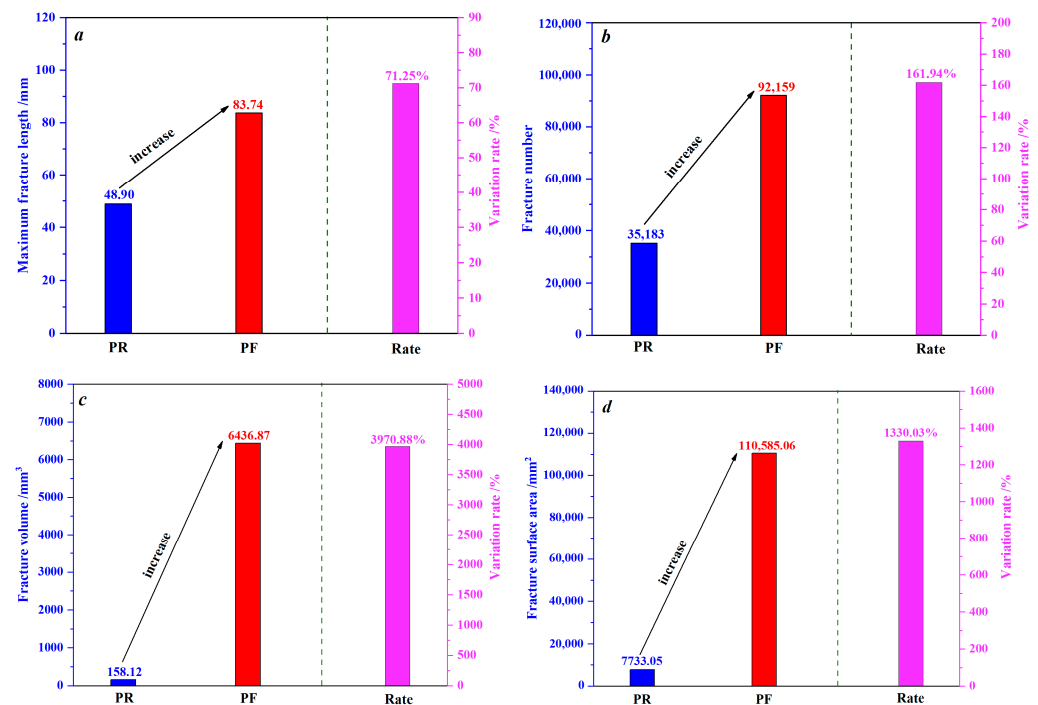


**Figure 7.** Variation of the 3D fracture structure parameters before and after CO<sub>2</sub>-PTF: (a) maximum fracture length, (b) fracture number, (c) fracture volume, (d) fracture surface area.

### 5. Discussion

#### 5.1. 3D Fracture Evolution Characteristics of Coal Induced by CO<sub>2</sub>-PTF

Figure 8 shows that after CO<sub>2</sub>-PTF, the fracture volume and surface area with a fracture length less than 0.14 mm decreased, and the fracture volume and surface area with a length greater than 0.14 mm increased. Figure 9 further indicates that after CO<sub>2</sub>-PTF, the fracture volume with a fracture length less than 0.14 mm decreases from 5.78 mm<sup>3</sup> to 5.13 mm<sup>3</sup>, a decrease of 11.24% (Figure 9a). The fracture volume with a fracture length greater than 0.14 mm increases from 152.34 mm<sup>3</sup> to 6431.74 mm<sup>3</sup>, an increase of 4121.96% (Figure 9b). After CO<sub>2</sub>-PTF, the fracture surface area with a fracture length of less than 0.14 mm decreases from 650.29 mm<sup>2</sup> to 593.06 mm<sup>2</sup>, a decrease of 8.80% (Figure 9c). The fracture surface area with a fracture length greater than 0.14 mm increases from 7082.76 mm<sup>2</sup> to 109,992.00 mm<sup>2</sup>, an increase of 1452.95% (Figure 9d).

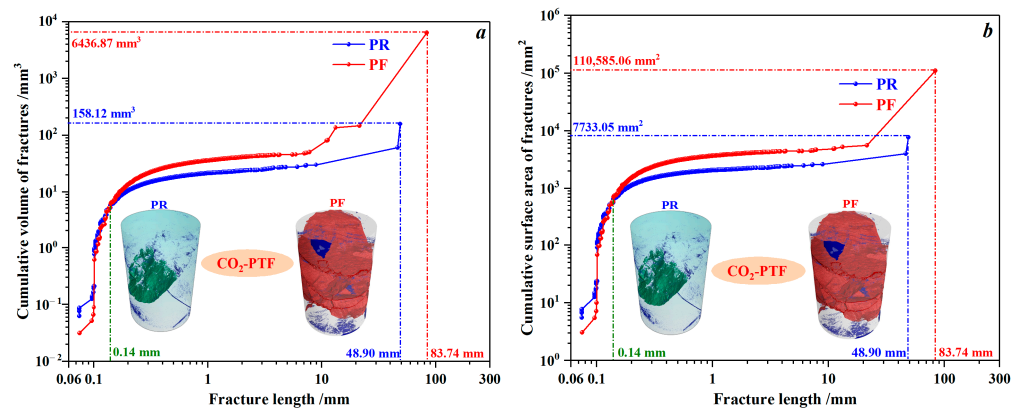


**Figure 8.** Evolution of 3D fracture volume and surface area: (a) cumulative volume of fracture, (b) cumulative surface area of fracture.

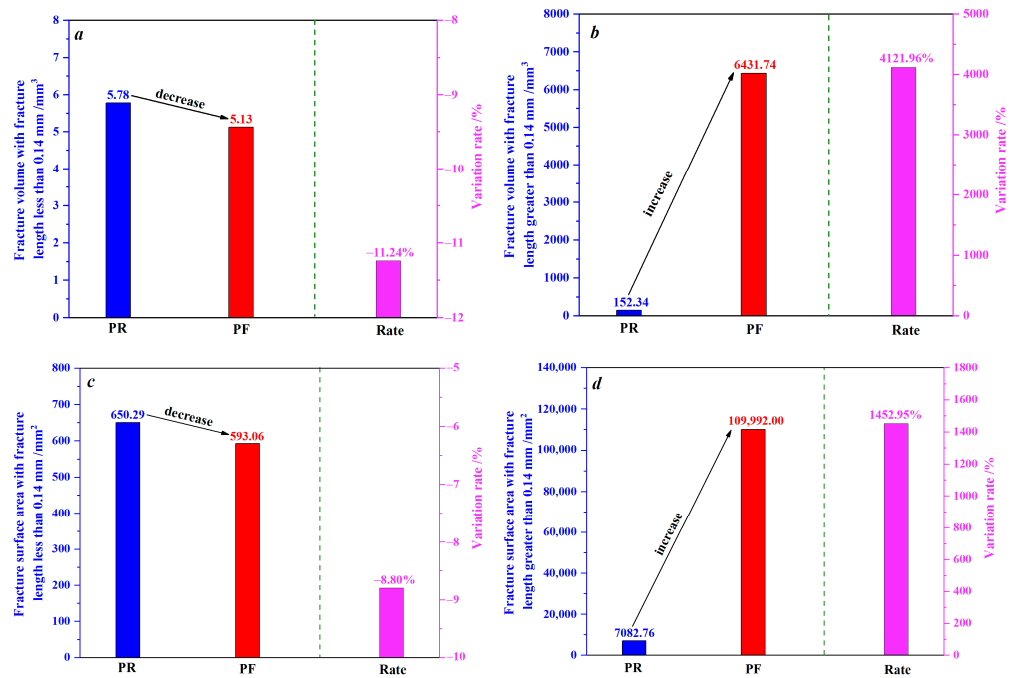


**Figure 9.** Comparison of fracture volume and surface area with the fracture length 0.14mm as the boundary: (a) fracture volume with fracture length less than 0.14 mm, (b) fracture volume with fracture length greater than 0.14 mm, (c) fracture surface area with fracture length less than 0.14 mm, (d) fracture surface area with fracture length greater than 0.14 mm.

The above fracture structure variation indicates that CO<sub>2</sub>-PTF promotes the expansion transformation of fractures with a length less than 0.14 mm into fractures with a length greater than 0.14 mm. In addition to the expansion transformation from the fractures with a length less than 0.14 mm, it is mainly due to the CO<sub>2</sub>-PTF generating a large number of new fractures with a length greater than 0.14 mm in coal. Therefore, the fracture evolution caused by CO<sub>2</sub>-PTF coal has dual effects, which are the fracture generation effect and fracture expansion-transformation effect, and the boundary between the dual effects of CO<sub>2</sub>-PTF coal under the fracturing pressure of 185 MPa is 0.14 mm (140 μm).

The fracture structure evolution induced by CO<sub>2</sub>-PTF coal is closely related to the process of CO<sub>2</sub>-PTF coal (Figure 10). The process of CO<sub>2</sub>-PTF coal is mainly divided into two stages: the early dynamic high-pressure gas jet stage and the subsequent quasi-static high-pressure gas stage [43–45]. In the early dynamic high-pressure gas jet stage, the high-pressure CO<sub>2</sub> gas jet is ejected from the discharge port and acts on the surrounding coal, forming a large number of new fractures. This stage corresponds to the fracture generation effect.

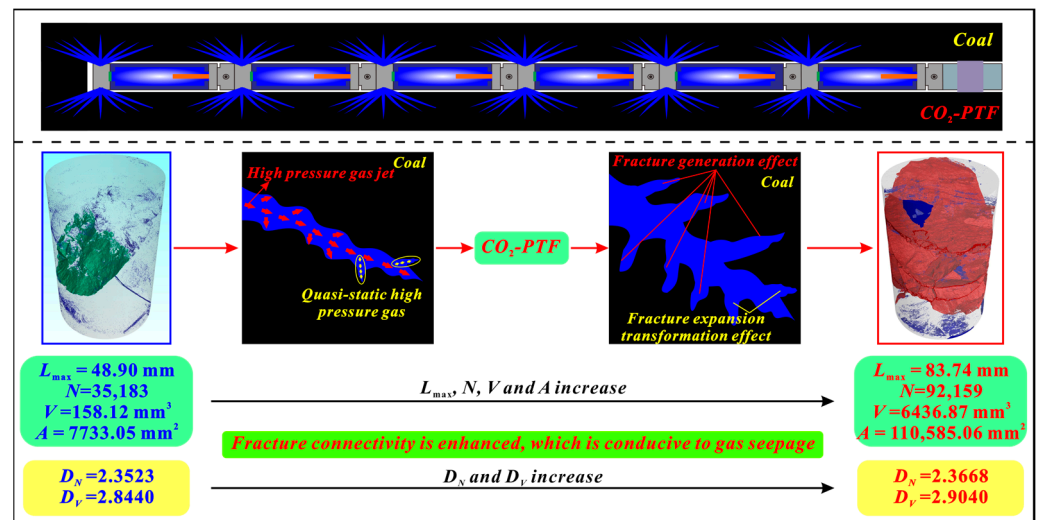


Figure 10. 3D fracture evolution of CO<sub>2</sub>-PTF coal.

The high-pressure CO<sub>2</sub> gas jet migrates along the fracture in coal and the CO<sub>2</sub> gas pressure decays, entering the subsequent quasi-static high-pressure gas stage. The CO<sub>2</sub> gas pressure is generally 5–8 MPa, which is much greater than the tensile strength of coal (0.5–1.5 MPa) [46], the “gas wedge effect” of high-pressure CO<sub>2</sub> gas will cause micro-fracture to expand and transform [47,48], resulting in the fracture expansion-transformation effect.

The fracture dual evolution effect (the fracture generation effect and fracture expansion-transformation effect) induced by CO<sub>2</sub>-PTF coal, especially the fracture generation effect, promotes a significant increase in the fracture number, volume and surface area, which causes the enhanced connectivity between fractures, and the increase in fractal dimensions for the fracture number and volume. In summary, CO<sub>2</sub>-PTF coal enhances the connectivity between fractures and provides an effective channel for gas seepage, which is conceived in the CBM drainage.

## 5.2. Potential Application in Evaluating the Effect of CO<sub>2</sub>-PTF Coal

According to this study, combining the fractal dimension  $D_V$  for fracture volume with the fractal dimension  $D_N$  for fracture number can more comprehensively reflect the connectivity evolution characteristics for the fracture structure of CO<sub>2</sub>-PTF coal. Therefore, we propose evaluation indicators to evaluate the 3D fracture evolution in coal caused by CO<sub>2</sub>-PTF from the perspectives of Euclidean geometry and fractal geometry, which mainly includes the maximum fracture length ( $L_{max}$ ), fracture volume ( $V$ ), the fracture number

( $N$ ), the fractal dimension ( $D_V$ ) for fracture volume and the fractal dimension ( $D_N$ ) for fracture number.

The fracture length reflects the fracture expansion range, so the larger the maximum fracture length ( $L_{\max}$ ), the larger the fracture expansion range. The fracture volume ( $V$ ), fracture number ( $N$ ), fractal dimension ( $D_V$ ) for fracture volume and fractal dimension ( $D_N$ ) for fracture number can represent the fracture connectivity [39,49–52]. The larger these values, the better the connectivity between fractures. The comprehensive evaluation diagram of five indicators for evaluating the 3D fracture evolution of CO<sub>2</sub>-PTF coal is shown in Figure 11.

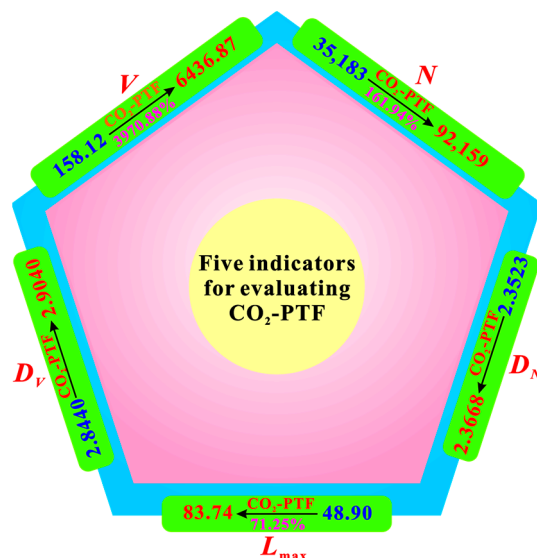


Figure 11. Five indicators for evaluating the 3D fracture evolution of CO<sub>2</sub>-PTF coal.

This research further reveals the fracture evolution mechanism by CO<sub>2</sub>-PTF coal and provides a new evaluation and analysis indicators for the effect of CO<sub>2</sub>-PTF. In addition, the above research method can provide theoretical and methodological references for the study of fracture evolution characteristics of other unconventional natural gas reservoirs and their reservoir stimulation.

## 6. Conclusions

According to the CT scanning technology and fractal theory, the variations in the length, number, volume and surface area of the 3D fractures in coal before and after CO<sub>2</sub>-PTF under the fracturing pressure of 185 MPa are analyzed. The fractal dimension ( $D_N$ ) for fracture number and fractal dimension ( $D_V$ ) for fracture volume before and after CO<sub>2</sub>-PTF are calculated. The fractal evolution characteristics of the 3D fracture structure of coal induced by CO<sub>2</sub>-PTF are revealed. The main conclusions are as follows:

CO<sub>2</sub> phase transition fracturing coal has the fracture generation effect and fracture expansion-transformation effect, causing the maximum fracture length to increase from 48.90 mm to 83.74 mm, the fracture number to increase from 35,183 to 92,159, the fracture volume to increase from 158.12 mm<sup>3</sup> to 6436.87 mm<sup>3</sup>, and the fracture surface area to increase from 7733.05 mm<sup>2</sup> to 110,585.06 mm<sup>2</sup>.

After CO<sub>2</sub>-PTF, the fractal dimension for fracture number increases from 2.3523 to 2.3668, and the fractal dimension for fracture volume increases from 2.8440 to 2.9040, which reflects the increased connectivity between three-dimensional fractures.

The volume and surface area of fractures with a length of less than 140 μm are reduced under the influence of the fracture expansion-transformation effect. The fracture expansion-transformation effect and fracture generation effect jointly promote a significant increase in the volume and surface area of fractures with a length greater than 140 μm. The

140  $\mu\text{m}$  is the critical value for the fracture expansion-transformation effect and fracture generation effect.

The early dynamic high-pressure gas jet stage of CO<sub>2</sub>-PTF coal promotes the generation of 3D fractures, and the subsequent quasi-static high-pressure gas stage promotes the expansion transformation of 3D fractures.

We proposed the five indicators to evaluate the 3D fracture evolution characteristics in coal caused by CO<sub>2</sub>-PTF, which can provide theoretical and methodological references for researching the fracture evolution characteristics of other unconventional natural gas reservoirs and their reservoir stimulation.

**Author Contributions:** Conceptualization, G.L. and P.C.; Data Curation, Z.Z., J.L. and G.B.; Formal Analysis, Z.Z., J.L. and G.B.; Funding Acquisition, G.L.; Methodology, Z.Z., J.L., G.B. and P.C.; Supervision, G.L. and P.C.; Visualization, Z.Z.; Writing—Original Draft, Z.Z. and G.L.; Writing—Review and Editing, G.L. and P.C. All authors have read and agreed to the published version of the manuscript.

**Funding:** This research was supported by the National Natural Science Foundation of China (No. 42230814 and No. 42372204), the China Scholarship Council (No. 202308410549), the Henan Province International Science and Technology Cooperation Project (No. 242102520034), the Henan Province Science and Technology Research Project (No. 242102320365) and the Key Research Projects of Higher Education Institutions in Henan Province (No. 24B170005).

**Data Availability Statement:** The data presented in this study are available from the corresponding author upon request.

**Conflicts of Interest:** The authors declare no conflicts of interest.

## Abbreviations

CO <sub>2</sub> -PTF	CO <sub>2</sub> phase transition fracturing
CT	Computed Tomography
CO <sub>2</sub> -PTF coal	CO <sub>2</sub> phase transition fracturing coal
CBM	coalbed methane
SEM	Scanning Electron Microscope
2D	two-dimensional
3D	three-dimensional
DM	damage mark
FRW	four-radial-wing fractures
TRW	tri-radial-wing fractures
$\Phi$	coal pillar diameter
$L_i$	fracture length
$N(L_i)$	the number of fractures with a fracture length greater than $L_i$
$C_1$	fitting constant
$D_N$	fractal dimension for fracture number
$A$	the surface area of the fracture
$V$	the volume of the fracture
$D_V$	fractal dimension for the 3D fracture volume
$C_2$	fitting constant
$N$	fracture number
$L_{\text{max}}$	the maximum fracture length

## References

- Lu, Y.; Zhang, H.; Zhou, Z.; Ge, Z.; Chen, C.; Hou, Y.; Ye, M. Current status and effective suggestions for efficient exploitation of coalbed methane in China: A review. *Energy Fuels* **2021**, *35*, 9102–9123. [[CrossRef](#)]
- Wang, X.; Zhou, F.; Ling, Y.; Xiao, Y.; Ma, B.; Ma, X.; Yu, S.; Liu, H.; Wei, K.; Kang, J. Overview and outlook on utilization technologies of low-concentration coal mine methane. *Energy Fuels* **2021**, *35*, 15398–15423. [[CrossRef](#)]
- Allen, D.T.; Chen, Q.; Dunn, J.B. Consistent metrics needed for quantifying methane emissions from upstream oil and gas operations. *Environ. Sci. Technol. Lett.* **2021**, *8*, 345–349. [[CrossRef](#)]
- Cheng, Y.; Pan, Z. Reservoir properties of Chinese tectonic coal: A review. *Fuel* **2020**, *260*, 116350. [[CrossRef](#)]

5. Liu, G.; Liu, H.; Xian, B.; Gao, D.; Wang, X.; Zhang, Z. Fuzzy pattern recognition model of geological sweetspot for coalbed methane development. *Pet. Explor. Dev.* **2023**, *50*, 924–933. [[CrossRef](#)]
6. Sampath, K.; Perera, M.; Ranjith, P.; Matthai, S.; Rathnaweera, T.; Zhang, G.; Tao, X. CH<sub>4</sub>-CO<sub>2</sub> gas exchange and supercritical CO<sub>2</sub> based hydraulic fracturing as CBM production-accelerating techniques: A review. *J. CO<sub>2</sub> Util.* **2017**, *22*, 212–230. [[CrossRef](#)]
7. Yuan, L. Control of coal and gas outbursts in Huainan mines in China: A review. *J. Rock Mech. Geotech. Eng.* **2016**, *8*, 559–567. [[CrossRef](#)]
8. Zhou, F.; Xia, T.; Wang, X.; Zhang, Y.; Sun, Y.; Liu, J. Recent developments in coal mine methane extraction and utilization in China: A review. *J. Nat. Gas Sci. Eng.* **2016**, *31*, 437–458. [[CrossRef](#)]
9. Weir, P.; Edwards, J. Mechanical loading and Cardox revolutionize an old mine. *Coal Age* **1928**, *33*, 288–290.
10. Singh, S. Non-explosive applications of the PCF concept for underground excavation. *Tunn. Undergr. Space Technol.* **1998**, *13*, 305–311. [[CrossRef](#)]
11. Dong, Q.; Wang, Z.; Han, Y.; Sun, X. Research on TNT equivalent of liquid CO<sub>2</sub> phase-transition fracturing. *China Saf. Sci. J.* **2014**, *24*, 84–88.
12. Lu, T.; Wang, Z.; Yang, H.; Yuan, P.; Han, Y.; Sun, X. Improvement of coal seam gas drainage by under-panel cross-strata stimulation using highly pressurized gas. *Int. J. Rock Mech. Min. Sci.* **2015**, *77*, 300–312. [[CrossRef](#)]
13. Chen, H.; Wang, Z.; Chen, X.; Chen, X.; Wang, L. Increasing permeability of coal seams using the phase energy of liquid carbon dioxide. *J. CO<sub>2</sub> Util.* **2017**, *19*, 112–119. [[CrossRef](#)]
14. Mojid, M.R.; Negash, B.M.; Abdulelah, H.; Jufar, S.R.; Adewumi, B.K. A state-of-art review on waterless gas shale fracturing technologies. *J. Pet. Sci. Eng.* **2021**, *196*, 108048. [[CrossRef](#)]
15. Cai, Y.; Liu, D.; Pan, Z.; Yao, Y.; Li, J.; Qiu, Y. Pore structure and its impact on CH<sub>4</sub> adsorption capacity and flow capability of bituminous and subbituminous coals from Northeast China. *Fuel* **2013**, *103*, 258–268. [[CrossRef](#)]
16. Moore, T.A. Coalbed methane: A review. *Int. J. Coal Geol.* **2012**, *101*, 36–81. [[CrossRef](#)]
17. Mohanty, M.M.; Pal, B.K. Sorption behavior of coal for implication in coal bed methane an overview. *Int. J. Min. Sci. Technol.* **2017**, *27*, 307–314. [[CrossRef](#)]
18. Bai, X.; Zhang, D.; Zeng, S.; Zhang, S.; Wang, D.; Wang, F. An enhanced coalbed methane recovery technique based on CO<sub>2</sub> phase transition jet coal-breaking behavior. *Fuel* **2020**, *265*, 116912. [[CrossRef](#)]
19. Xia, B.; Liu, X.; Song, D.; He, X.; Yang, T.; Wang, L. Evaluation of liquid CO<sub>2</sub> phase change fracturing effect on coal using fractal theory. *Fuel* **2021**, *287*, 119569. [[CrossRef](#)]
20. Liu, H.; Liu, G.; Zhang, Z.; Li, B.; Si, N.; Guan, W.; Lin, J. Effects of Liquid CO<sub>2</sub> Phase Transition Fracturing on Mesopores and Micropores in Coal. *Energy Fuels* **2022**, *36*, 10016–10025. [[CrossRef](#)]
21. Cao, Y.; Zhang, J.; Zhai, H.; Fu, G.; Tian, L.; Liu, S. CO<sub>2</sub> gas fracturing: A novel reservoir stimulation technology in low permeability gassy coal seams. *Fuel* **2017**, *203*, 197–207. [[CrossRef](#)]
22. Cao, Y.; Zhang, J.; Zhang, X.; Liu, S.; Elsworth, D. Micro-fractures in coal induced by high pressure CO<sub>2</sub> gas fracturing. *Fuel* **2022**, *311*, 122148. [[CrossRef](#)]
23. Liu, X.; Wang, Z.; Song, D.; He, X.; Yang, T. Variations in surface fractal characteristics of coal subjected to liquid CO<sub>2</sub> phase change fracturing. *Int. J. Energy Res.* **2020**, *44*, 8740–8753. [[CrossRef](#)]
24. Liao, Z.; Liu, X.; Song, D.; He, X.; Nie, B.; Yang, T.; Wang, L. Micro-structural damage to coal induced by liquid CO<sub>2</sub> phase change fracturing. *Nat. Resour. Res.* **2021**, *30*, 1613–1627. [[CrossRef](#)]
25. Laubach, S.; Marrett, R.; Olson, J.; Scott, A. Characteristics and origins of coal cleat: A review. *Int. J. Coal Geol.* **1998**, *35*, 175–207. [[CrossRef](#)]
26. Wang, Z.; Pan, J.; Hou, Q.; Yu, B.; Li, M.; Niu, Q. Anisotropic characteristics of low-rank coal fractures in the Fukang mining area, China. *Fuel* **2018**, *211*, 182–193. [[CrossRef](#)]
27. Huy, P.Q.; Sasaki, K.; Sugai, Y.; Ichikawa, S. Carbon dioxide gas permeability of coal core samples and estimation of fracture aperture width. *Int. J. Coal Geol.* **2010**, *83*, 1–10. [[CrossRef](#)]
28. Liu, P.; Nie, B.; Zhao, Z.; Zhao, Y.; Li, Q. Characterization of ultrasonic induced damage on multi-scale pore/fracture in coal using gas sorption and  $\mu$ -CT 3D reconstruction. *Fuel* **2023**, *332*, 126178. [[CrossRef](#)]
29. Wang, X.; Pan, J.; Wang, K.; Mou, P.; Li, J. Fracture variation in high-rank coal induced by hydraulic fracturing using X-ray computer tomography and digital volume correlation. *Int. J. Coal Geol.* **2022**, *252*, 103942. [[CrossRef](#)]
30. Liu, G.; Zhang, Z.; Cao, Y.; Wang, X.; Liu, H.; Li, B.; Si, N.; Guan, W. An Analogical Method on Fractal Dimension for Three-Dimensional Fracture Tortuosity in Coal Based on Ct Scanning. *Fractals* **2023**, *31*, 2350072. [[CrossRef](#)]
31. Mazumder, S.; Wolf, K.-H.; Elewaut, K.; Ephraim, R. Application of X-ray computed tomography for analyzing cleat spacing and cleat aperture in coal samples. *Int. J. Coal Geol.* **2006**, *68*, 205–222. [[CrossRef](#)]
32. Mathews, J.P.; Campbell, Q.P.; Xu, H.; Halleck, P. A review of the application of X-ray computed tomography to the study of coal. *Fuel* **2017**, *209*, 10–24. [[CrossRef](#)]
33. Karacan, C.; Okandan, E. Adsorption and gas transport in coal microstructure: Investigation and evaluation by quantitative X-ray CT imaging. *Fuel* **2001**, *80*, 509–520. [[CrossRef](#)]
34. Zhang, Z.; Liu, G.; Chang, P.; Wang, X.; Lin, J. Fractal characteristics for coal chemical structure: Principle, methodology and implication. *Chaos Solitons Fractals* **2023**, *173*, 113699. [[CrossRef](#)]
35. Yu, B. Analysis of flow in fractal porous media. *Appl. Mech. Rev.* **2008**, *61*, 050801. [[CrossRef](#)]

36. Zhang, Z.; Liu, G.; Wang, X.; Lv, R.; Liu, H.; Lin, J.; Barakos, G.; Chang, P. A fractal Langmuir adsorption equation on coal: Principle, methodology and implication. *Chem. Eng. J.* **2024**, *488*, 150869. [[CrossRef](#)]
37. Fu, Y.; Chen, X.; Feng, Z. Characteristics of coal-rock fractures based on CT scanning and its influence on failure modes. *J. China Coal Soc.* **2020**, *45*, 568–578.
38. Roy, A.; Perfect, E.; Dunne, W.M.; McKay, L.D. Fractal characterization of fracture networks: An improved box-counting technique. *J. Geophys. Res. Solid Earth* **2007**, *112*, B12201. [[CrossRef](#)]
39. Zhang, Z.; Liu, G.; Wang, X.; Li, B.; Liu, H. Fractal Characterization On Fracture Volume In Coal Based On Ct Scanning: Principle, Methodology, And Implication. *Fractals* **2022**, *30*, 2250124. [[CrossRef](#)]
40. Du, F.; Wang, K.; Zhang, G.; Zhang, Y.; Zhang, G.; Wang, G. Damage characteristics of coal under different loading modes based on CT three-dimensional reconstruction. *Fuel* **2022**, *310*, 122304. [[CrossRef](#)]
41. Sun, L.; Zhang, C.; Wang, G.; Huang, Q.; Shi, Q. Research on the evolution of pore and fracture structures during spontaneous combustion of coal based on CT 3D reconstruction. *Energy* **2022**, *260*, 125033. [[CrossRef](#)]
42. Zhang, K.; Wang, S.; Wang, L.; Cheng, Y.; Li, W.; Han, X.; Liu, C.; Su, H. 3D visualization of tectonic coal microstructure and quantitative characterization on topological connectivity of pore-fracture networks by Micro-CT. *J. Pet. Sci. Eng.* **2022**, *208*, 109675. [[CrossRef](#)]
43. Shang, Z.; Wang, H.; Li, B.; Cheng, Y.; Zhang, X.; Wang, Z.; Geng, S.; Wang, Z.; Chen, P.; Lv, P. The effect of leakage characteristics of liquid CO<sub>2</sub> phase transition on fracturing coal seam: Applications for enhancing coalbed methane recovery. *Fuel* **2022**, *308*, 122044. [[CrossRef](#)]
44. Zhang, Y.; Deng, H.; Ke, B.; Gao, F. Research on the explosion effects and fracturing mechanism of liquid carbon dioxide blasting. *Min. Metall. Explor.* **2022**, *39*, 521–530. [[CrossRef](#)]
45. Shang, Z.; Wang, H.; Li, B.; Cheng, Y.; Zhang, X.; Zhao, F.; Zhang, X.; Hao, C.; Wang, Z. Fracture processes in coal measures strata under liquid CO<sub>2</sub> phase transition blasting. *Eng. Fract. Mech.* **2021**, *254*, 107902. [[CrossRef](#)]
46. Cao, Y.; Zhang, J.; Tian, L.; Zhai, H.; Fu, G.; Tang, J. Research and application of CO<sub>2</sub> gas fracturing for gas control in low permeability coal seams. *J. China Coal Soc.* **2017**, *42*, 2631–2641.
47. Yang, R.; Ding, C.; Yang, L.; Lei, Z.; Zhang, Z.; Wang, Y. Visualizing the blast-induced stress wave and blasting gas action effects using digital image correlation. *Int. J. Rock Mech. Min. Sci.* **2018**, *112*, 47–54. [[CrossRef](#)]
48. Li, Y.; Ji, H.; Li, G.; Hu, S.; Liu, X. Effect of supercritical CO<sub>2</sub> transient high-pressure fracturing on bituminous coal microstructure. *Energy* **2023**, *282*, 128975. [[CrossRef](#)]
49. Wang, D.; Zeng, F.; Wei, J.; Zhang, H.; Wu, Y.; Wei, Q. Quantitative analysis of fracture dynamic evolution in coal subjected to uniaxial and triaxial compression loads based on industrial CT and fractal theory. *J. Pet. Sci. Eng.* **2021**, *196*, 108051. [[CrossRef](#)]
50. Karra, S.; O'Malley, D.; Hyman, J.; Viswanathan, H.S.; Srinivasan, G. Modeling flow and transport in fracture networks using graphs. *Phys. Rev. E* **2018**, *97*, 033304. [[CrossRef](#)]
51. Jafari, A.; Babadagli, T. Estimation of equivalent fracture network permeability using fractal and statistical network properties. *J. Pet. Sci. Eng.* **2012**, *92*, 110–123. [[CrossRef](#)]
52. Miao, T.J.; Yu, B.M.; Duan, Y.G.; Fang, Q.T. A fractal analysis of permeability for fractured rocks. *Int. J. Heat Mass Transf.* **2015**, *81*, 75–80. [[CrossRef](#)]

**Disclaimer/Publisher's Note:** The statements, opinions and data contained in all publications are solely those of the individual author(s) and contributor(s) and not of MDPI and/or the editor(s). MDPI and/or the editor(s) disclaim responsibility for any injury to people or property resulting from any ideas, methods, instructions or products referred to in the content.